Journal of Materials Chemistry C

Accepted Manuscript

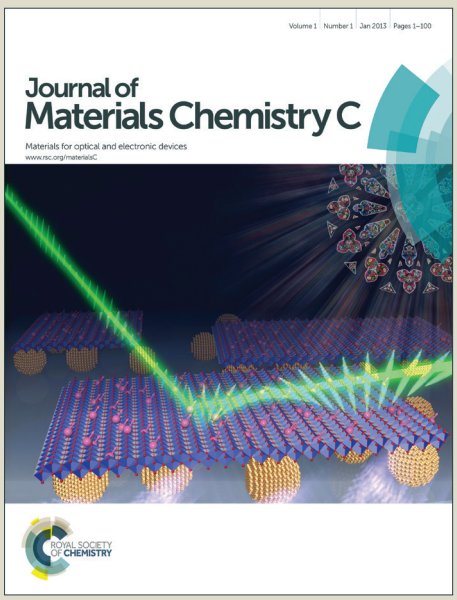

ROYAL SOCIETY OF CHEMISTRY

www.rsc.org/materialsC

Journal of Materials Chemistry C

RSCPublishing

ARTICLE

The Sb_2O_3 redox route to obtain copper nanoparticles in glasses with plasmonic properties†

Cite this: DOI: 10.1039/x0xx00000x

Douglas F. Franco[a], Antonio C. Sant'Ana,[a] Luiz F. C. De Oliveira[a] and Mauricio A. P. Silva[a]

Received 00th January 2012,
Accepted 00th January 2012

DOI: 10.1039/x0xx00000x

www.rsc.org/

A new route for production of oxide glasses containing copper nanoparticles was explored. The *antimony (III) oxide redox route* allowed the use of the reducing properties of α-Sb_2O_3, during melting, to decrease the oxidation number of copper ions in the glassy matrix. Such glasses have different Cu^{II}/Cu^{I} ratio in their composition as well as metallic copper nanoparticles with different size distributions, depending on Sb_2O_3 content. The electronic spectrum of the $0.3NaPO_3$-$0.6Sb_2O_3$-0.1CuO glass showed a band at 585 nm assigned to the localized surface plasmon resonance transition from copper nanoparticles, which is very important property for surface-enhanced spectroscopies. Raman spectroscopy studies of these glasses showed that the short range structure around Sb atoms is closely related to the high temperature β-Sb_2O_3 phase. Upon heating, α-Sb_2O_3 → α-Sb_2O_4 → β-Sb_2O_4 → β-Sb_2O_3 phase transitions occur with increasing temperatures. The short range structures of the glass-forming liquid and the resulting glass were shown to be related to the most stable phase at the melting temperature. Surface enhanced fluorescence spectra from Er^{III} ions, induced by the presence of copper nanoparticles, could be observed in doped glasses.

Introduction

The interaction of electromagnetic waves with metallic nanoparticles has attracted the attention of material science researchers due to their unique optical properties, which have evolved to the arising of a new optics field, named photonics.[1,2] The interaction of metals with low frequency electromagnetic radiation is characterized by reflection processes and do not allow electromagnetic waves to propagate through the metal. Under near-infrared and visible radiations, field penetration increases, leading to increased dissipation. At higher frequencies regimes, metals acquire dielectric character and allow the propagation of electromagnetic waves.[3] Alkali metals such as sodium have an almost free-electron-like response and thus exhibit an "ultraviolet transparency".[4] On the other hand, in this regime gold, silver or copper metallic nanoparticles have a coherent oscillation of the electrons from conduction band with the electromagnetic field, leading to a strong absorption.[1,5-6] This phenomenon is called "localized surface plasmon resonance" (LSPR) which allows sustain giant localized electrical fields in the interface of the metallic surface with the glassy dielectric matrix. Some applications of these nanostructured composites include surface-enhanced Raman scattering (SERS), surface enhanced fluorescence (SEF), surface plasmon resonance imaging and spectroscopy, with technological applications as solid-state lasers, memory and display devices, dichroic polarizers, optical amplifiers and sensors, colored glasses, ophthalmic lenses, optoelectronic materials, etc.[7-13]

Metal-glass nanostructured composites are among the systems bearing relevant interest in photonics. The use of glasses as dielectric matrix hosts for both metallic nanoparticles and rare-earth (RE) ions has some advantages over other systems, such as high transparency in selective electromagnetic fields, mechanical and chemical strength (properties easily controlled with appropriate glass composition), possibility of production of devices on several shapes such as blocks, lenses and fibers and the absence of metal-ligand interactions, which would cause quenching processes due to the high energy stretching vibrations.[7,14] Heavy metal oxide (HMO) glasses are preferred over the traditional silicate, borate or phosphate glasses, due to their low phonon energy, which enhances the upconversion efficiency of RE ions by decreasing their multiphonon relaxation rate. Other important properties of HMO glasses include high refractive index, large transmission windows and large non-linear optical properties.[14,15] Antimony(III) oxide, Sb_2O_3, is a good low phonon energy HMO glass former.[16] Besides well studied in their optical and structural properties, it was not yet emphasized Sb_2O_3 undergoes phase transitions induced by heating. Moreover, these phase transitions are accompanied by oxidation processes $Sb^{III} \rightarrow Sb^{V} + 2e^-$, which certainly affects the glass structures, compositions and, consequently, their properties. Two known crystalline forms of antimony (III) oxide are the cubic α-Sb_2O_3, senarmontite, and the high temperature orthorhombic phase β-Sb_2O_3, valentinite. Upon heating at 500°C, senarmontite undergoes solid-solid phase transition accompanied by redox reactions, leading to the orthorhombic phase α-Sb_2O_4, known as cervantite. At around 700 °C, another phase transition takes place leading to the monoclinic β-Sb_2O_4 phase, known as clinocervantite. The unit cell of both α-Sb_2O_4 and β-Sb_2O_4 possess antimony atoms with (III) or (V) oxidation numbers. In such crystalline phases the number of coordinated oxygen atoms is four or six for Sb^{III} or Sb^{V}, respectively, with the tetrahedral and octahedral units linked through Sb^{III}–O–Sb^{V} bridges.[17-19] The direct production of glasses containing metallic nanoparticles using the conventional melting/quenching

technique is a difficult task mainly due to oxidation processes occurring at high temperatures during the melting of the precursors. This has led to the use of multi-step techniques for glass syntheses as sol-gel process, metal-glass co-sputtering deposition, metal-ion implantation, pulsed laser deposition, ion-exchange and extended heat treatments above the glass transition temperature (T_g) in reducing atmospheres.[4-16] In fact, glasses containing Sb_2O_3 as reduction agent were until now prepared only with silver and/or gold nanoparticles.[20] In this work, we explore the reduction potential of antimony oxide at high temperatures in order to obtain HMO glasses–copper nanoparticles composites directly from the melt, without any post-production process, such as heat treatments. As shown in this paper, the Sb_2O_3 redox route is an easy way to obtain glasses containing cupric and cuprous ions with different ratios as well as copper nanoparticles, imprinting important optical properties to these glasses.

Experimental section

Glasses in the $NaPO_3$-Sb_2O_3-CuO system were prepared from reagent grade sodium polyphosphate $NaPO_3$ (99%, Merck), antimony(III) oxide Sb_2O_3 (99%, Aldrich) and copper(II) oxide CuO (99,9%, Aldrich). The oxides were weighted considering the molar proportions of each sample, to give a total mass of 5.0 grams, finely grinded and homogenized in agate mortar and pestle and then melted in platinum crucibles at 1000 °C under atmospheric conditions. Melting time was maintained to a minimum acceptable, to avoid excessive loss of Sb_2O_3 on volatilization. Melt homogenization was made manually by crucible stirring and depending on the glass composition the melting time varied. First samples prepared, with low Sb_2O_3 and CuO concentrations, were kept in furnace for 10 minutes. The increase of Sb_2O_3 contents lead to an intense volatilization process and if the melting time is greater than 6 or 7 minutes the resultant material do not vitrifies. To increase the glass-forming composition range on this ternary system, glasses compositions with more than 80 mol% on Sb_2O_3 and 20 mol% on CuO were melted during 5 minutes. The melts were quenched between steel moulds and, depending on composition, blue, green, brown or black glasses of approximately 1 mm thickness were obtained.

In order to investigate the redox processes in these glasses, samples prepared with starting molar composition $(0.9\text{-}x)NaPO_3$–xSb_2O_3–0.1CuO, with $0.1 \leq x \leq 0.8$, were investigated through differential scanning calorimetry (DSC), X-ray diffraction (XRD), Raman scattering, electronic absorption or reflection (localized surface plasmon resonance - LSPR) and X-ray absorption near edge structure (Cu K-edge XANES) spectroscopies. The samples used for obtaining electronic spectra were prepared with good optical quality as follows: bulk glasses with dimensions *ca.* 2 x 1 x 0.5 cm were prepared using 10 grams of the melt, poured into pre heated molds at 300°C and annealed in this temperature for 12 hours, followed by slow cooling to room temperature. These samples were cut in 1 x 0.5 x 0.1 cm blocks and then polished before analysis. Glasses doped with 0.5 Mol% of Erbium (III) oxide were prepared with molar composition $(0.895\text{-}x)NaPO_3$–xSb_2O_3–0.1CuO–$0.005Er_2O_3$ with $x = 0.3$ and 0.6, for verifying RE surface enhanced fluorescence effect.

Thermal analysis were performed using a Schimadzu DSC60 calorimeter with a programmed heating rate of 10°Cmin^{-1} up to 550°C, under N_2 atmosphere, in aluminum crucibles. The reflectance spectra in visible region were obtained from an Ocean Optics USB2000 spectrometer, in the range 350–800 nm. Raman measurements were carried out using a Horiba XploRA instrument, equipped with air cooled charge-coupled device detector with the incident laser beam focused on the sample using a confocal microscope with a 50x objective and 2 cm^{-1} spectral resolution. The spectra were recorded using 532 nm excitation line, with 100 mW laser intensity. Fluorescence spectra were obtained with a $\lambda_{exc.}$ = 785 nm, with 10 s accumulation time and power laser of 10 mW. Cu K-edge XANES spectra were obtained in the XAFS-2 beam line at the Brazilian Synchrotron Light Laboratory (LNLS). For these experiments, finely powdered glasses (5μm) were mixed to boron nitride, pressed in 1 mm thick pellets and fixed between two Kapton® tapes. XRD measurements were performed on a D8 DaVinci diffractometer from Bruker, using the Cu Kα radiation (λ = 1.5418 Å) with LynxEye liner Position Sensitive Detector, Ni-filter and Bragg-Brentano geometry. The XRD data were collected in the 2θ range between 10 and 90° with step size of 0.01° and counting time of 0.5 seconds per step. The electronic absorption spectra were performed using a Schimadzu 1800 spectrometer with tungsten filament and deuterium sources. Fluorescence emission spectra were obtained from a Raman spectrometer Bruker SenTerra, coupled with an optical microscopy and using 785 nm excitation line.

Results and discussion

Figure 1 shows the pseudo-ternary glass forming composition diagram for the $NaPO_3$-Sb_2O_3-CuO system. A large glass-forming composition range is observed and glasses with CuO content as high as 30 %mol can be obtained. In this work $(0.9\text{-}x)NaPO_3$–xSb_2O_3–0.1CuO compositions, with $0.1 \leq x \leq 0.8$, were choose to be analyzed. It is important to observe that the glasses from $x = 0.1$ to 0.6 were obtained after 5 minutes at 1000°C (circles in Figure 1), while those with $x = 0.7$ and 0.8 were melted during 3 minutes (triangles in Figure 1). When Sb_2O_3 content is increased the color of the glasses varied from blue ($x = 0.1$) to green and then brown.

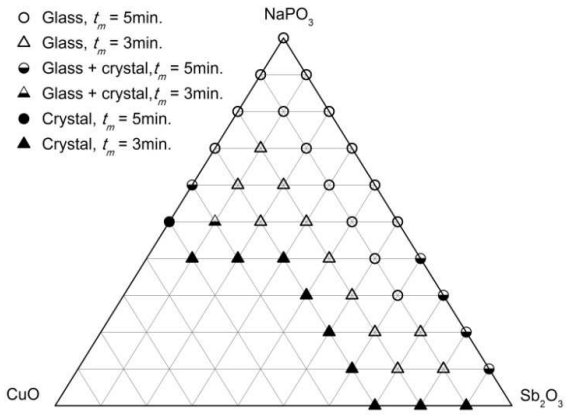

Figure 1. Glass-forming compositions diagram for the $NaPO_3$-Sb_2O_3-CuO system in molar fraction. t_m= melting time.

Figure 2 shows the reflectance spectra of the glasses obtained with different concentration of the Sb_2O_3 reducing agent. For $x = 0.1$ the low reflectance in the red and near-infrared regions, associated with the absorption of the radiation by the sample, and the relative high reflectance around 450-500 nm can be correlated with the apparent blue color of the sample. Increasing Sb_2O_3 concentration in the glasses, the maximum of the curves tends towards red, increasing the reflectance in the red, and near-infrared regions. This result is

coherent with the color changes (blue → green → brown) in these glasses. For instances, x = 0.7 has high reflectance in the near infrared with an extended tail in the visible region with low reflectance (high absorbance), resulting in the brown color of the material. It is well known that the blue and green colors are characteristic of Cu^{II} and Cu^{I} complexes respectively, while systems with metallic Cu colloidal nanoparticles possess brownish color.[21] This allows to infer that the reflectance patterns can be associated with the presence of copper species in different oxidation states, presenting different molar proportion between them.

Figure 3 shows DSC curves of the glasses, and in the inset of this figure the glass transition temperature T_g is plotted as a function of Sb_2O_3 molar fraction. Large undercooled melting temperature regions (T_x-T_g) are observed for these samples, attaining a maximum value of 180 °C for the x = 0.3 glass, composition which also presents the highest T_g value. Glass compositions with x > 0.3 present a decrease in the glass transition temperature with Sb_2O_3 content. Considering the relation between the glass transition temperature and the connectivity of the vitreous network, one can conclude that the addition of up to 30 mol% of Sb_2O_3 in the glass composition lead to the formation of bonding P-O-Sb species acting as glassy network formers, increasing the chain lengths and connectivity in the undercooled melt and, consequently, in the glass structure.

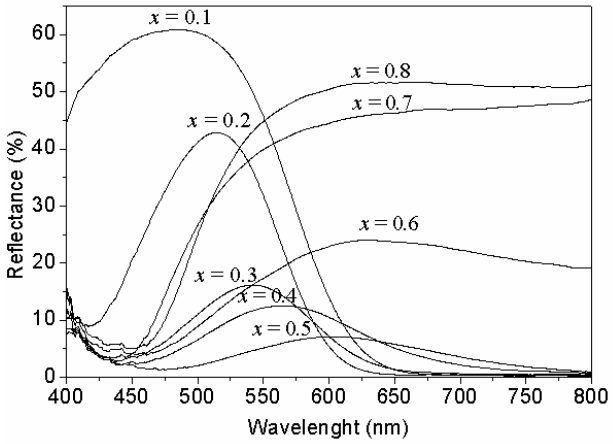

Figure 2. Reflectance spectra of the glasses with composition (0.9-x)$NaPO_3$-$x$$Sb_2O_3$-0.1CuO, from x = 0.1 to x = 0.8.

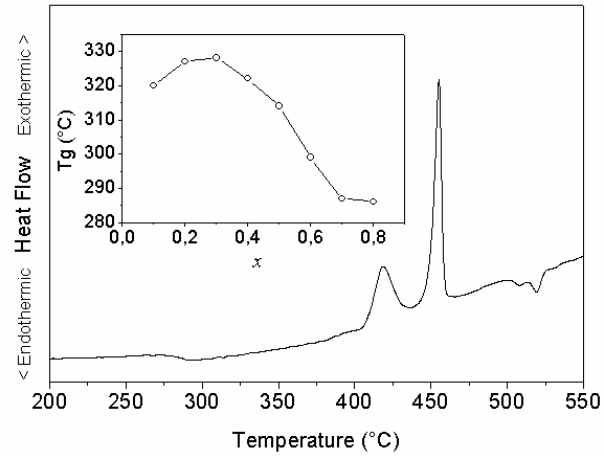

Figure 3: DSC curve of the 0.1$NaPO_3$-0.8Sb_2O_3-0.1CuO glass. Inset: Glass transition temperature (T_g) variation as a function of Sb_2O_3 molar fraction in the glasses (0.9-x)$NaPO_3$-$x$$Sb_2O_3$-0.1CuO.

For x > 0.3, the decrease on T_g values can be attributed to the inclusion of Sb atoms coordinated to terminal positions, leading to a decrease in the vitreous network lengths and connectivity.

Figure 4 shows the Raman spectra of the studied glasses and standards $NaPO_3$ and β-Sb_2O_3. The shifts and broadening of the Raman bands of glass samples indicate that the presence of Sb_2O_3 and CuO in the glassy $NaPO_3$ network strongly influences the vibrational characteristics of the resulting glasses.

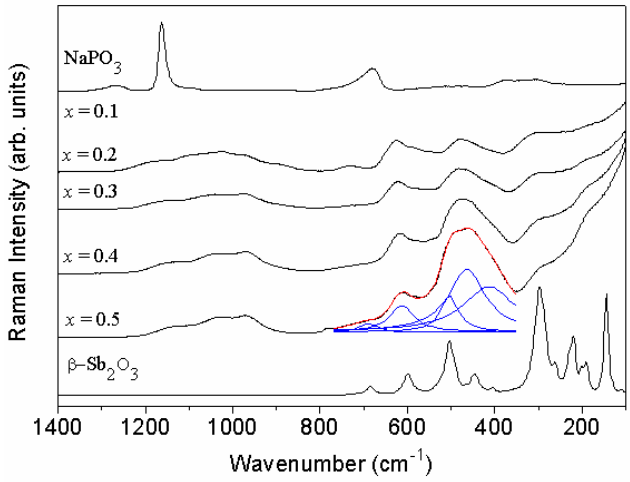

Figure 4: Raman spectra of the glasses (0.9-x)$NaPO_3$-$x$$Sb_2O_3$-0.1CuO and of standard samples of $NaPO_3$ and β-Sb_2O_3 (valentinite). Deconvolution of the Raman spectrum for x = 0.5 sample in the 770-350 cm^{-1} region is also shown.

The main Raman active vibrational modes of the polyphosphate chains are observed in glassy $NaPO_3$ as the bands at around 690 and 1160 cm^{-1}, assigned to the P-O-P symmetric stretching mode, from bonds involving two Q^2 species and PO_2 symmetric stretching from terminal P-O bonds in Q^2 species, ν_s(P-O_b) and ν_s(P-O_t), respectively.[22-24] These features are strongly damped in the glasses and several broad and low intensity bands appear in the region extending from 1300 to 700 cm^{-1}, ascribed as follows: the broad band centered at 1214 cm^{-1} is assigned to the asymmetric PO_2 stretching mode of terminal P-O bonds, ν_{as}(P-O_t), in Q^2 species; the band centered at 1121 cm^{-1} is assigned to the symmetric PO_2 stretching mode of terminal P-O bonds, ν_s(P-O_t), in Q^2 species; the shoulder at around 1080 cm^{-1} is due both to the symmetric PO_2 stretching mode, ν_s(P-O_t), in Q^2 species in polyphosphate groups and the asymmetric PO_3 stretching mode, ν_{as}(P-O_t), in Q^1 species in the polyphosphate and pyrophosphate groups; the band centered at 1030 and the shoulder at around 975 cm^{-1} are due to the symmetric PO_3 stretching modes, ν_s(P-O_t), in Q^1 species in the pyrophosphate and polyphosphate groups, respectively; the band centered at 888 cm^{-1} is assigned to the symmetric PO_4 stretching mode ν_s(P-O_t) in Q^0 species in the orthophosphate groups and asymmetric P-O-P vibration ν_{as}(P-O_b) and finally the band centered at 738 cm^{-1} can be assigned to both P-O-P symmetric stretching mode ν_s(P-O_b), between two Q^1 species or between one Q^1 and one Q^2 species and P-O-P symmetric stretching mode ν_s(P-O_b) between two Q^2 species.[22-24]

The frequency range at *ca.* 700-100 cm^{-1} in the Raman spectra of the glasses is dominated by the Sb_2O_3 vibrational modes.[19] Due to the amorphous nature of the samples, the broadening of these bands difficult a definitive assignment of the Raman spectra. Nevertheless,

it can be seen that the bands in this region increase in intensity with Sb_2O_3 content. The main feature in the Raman spectra of different glasses is the broad band centered at around 500 cm^{-1} which has relative intensity dramatically enhanced with Sb_2O_3 content. The deconvolution of the Raman bands at *ca.* 800-400 cm^{-1}, in the spectrum of $x = 0.5$ glass, shows peaks in position comparable with those present in the Raman spectrum of the valentinite phase β-Sb_2O_3, at 598, 504, 445 and 405 cm^{-1}. The peak at 297 cm^{-1} in the valentinite Raman spectrum also corresponds perfectly with the position of the shoulder present in all spectra of studied glasses. The band at 598 cm^{-1} is assigned to the symmetric and asymmetric combination of stretching vibrations ν_{asym} (Sb→O→Sb), while the bands centered at 504 and 445 cm^{-1} are assigned to the symmetric and asymmetric combination of Sb-O-Sb vibration. The band at 297 cm^{-1} is assigned to the symmetric and asymmetric combination of scissoring δ (Sb–O).[19] In this work, the crystalline standard β-Sb_2O_3 sample was obtained after the fast quenching of the Sb_2O_3 melt at 1000 °C. The glasses were also obtained via quenching of the melt at 1000 °C. Since the glass structures are closely related to the structures of the corresponding liquids, it is expected that in these glasses the local structure around Sb atoms is similar to that present in the corresponding high temperature phase. The deconvolution of the Raman spectrum of the $x = 0.5$ glass in fact indicates that the short range ordering around the antimony atoms reflects the presence of the high temperature valentinite phase. The phase transitions related to the oxidation of Sb species ($Sb^{III} \rightarrow Sb^{V} + 2e^-$) occurs at lower temperatures, i.e. in the 500-800°C range, which ensures the reduction of copper ions takes place during the melting process.

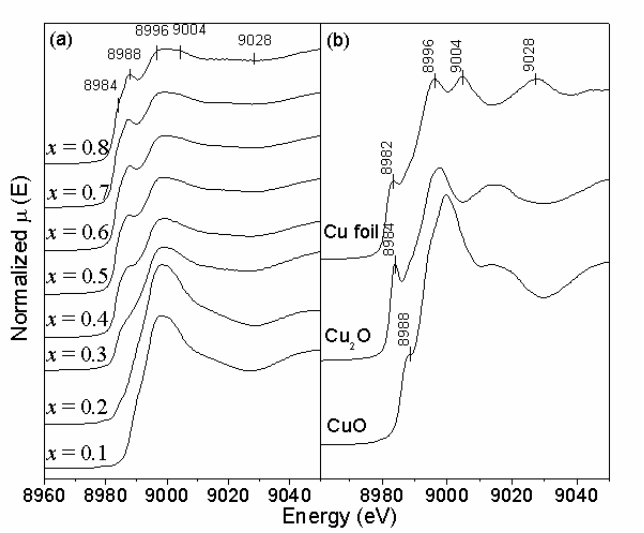

Figure 5: Cu K-edge XANES spectra of the (0.9-*x*)$NaPO_3$-*x*Sb_2O_3-0.1CuO glasses (a) and reference compounds (b).

Figure 5 shows the normalized Cu K-edge XANES spectra of the glasses (a) and the reference compounds CuO, Cu_2O and metallic Cu foil (b). The energy values of some of the main features for all glass samples and standard materials are shown in these spectra. The shift of the absorption edge to smaller energy values is known to be related to the decrease of oxidation number of the absorbing atom.[25] By comparing the edge profiles in the XANES spectra of glasses and references, it is clear that the increase of the molar proportion of Sb_2O_3 in the glass composition leads to the progressive decrease of the predominant oxidation number of copper atoms from Cu^{II} to Cu^{I} and Cu^0 in the glassy matrix. The profiles of the absorption edges of the samples show that both cupric and cuprous ions, as well as metallic copper, are present in the glasses with higher Sb_2O_3 content.

The presence of metallic copper and crystalline Cu_2O in the glasses with higher Sb_2O_3 content is confirmed through X-ray diffraction measurements, as shown in Figure 6.

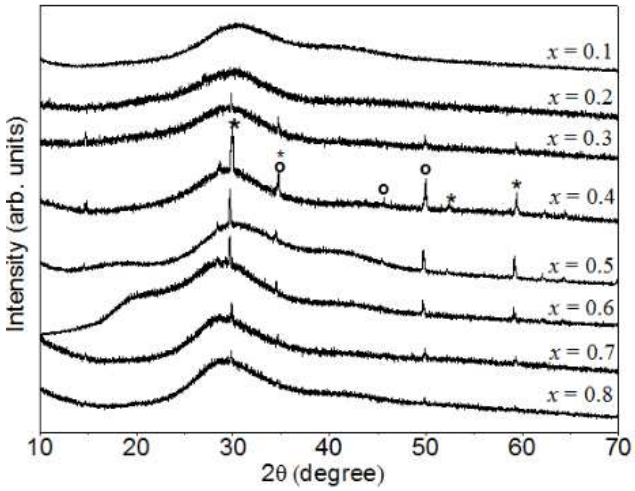

Figure 6: X-ray powder diffraction patterns of the (0.9-*x*)$NaPO_3$-*x*Sb_2O_3-0.1CuO glasses. Asterisks: Cu_2O (JCPDS#78-2076); circles: metallic Cu (JCPDS#04-0836).

While the glasses present the expected amorphous halo in the diffraction pattern, samples with $x \geq 0.3$ present diffraction peaks as 2θ = 34.8° (1 1 0), 45.7° (1 1 1) and 50.8° (2 0 0), attributed to the face-centered cubic phase of metallic copper (*Fm3m, a* = 3.615 Å, JCPDS file number 04-0836, indicated by circles in Figure 6). Other diffraction peaks are observed at 2θ = 29.9º (1 1 0), 34.8° (1 1 1), 42.4° (2 0 0), 52.4° (2 1 1) and 59.4° (2 2 0) and can be readily indexed to the cubic cuprite structure of cuprous oxide (*Pn3m, a* = 4.267 Å, JCPDS file number 78-2076, marked with asterisks in Figure 6). The presence of diffraction patterns of both Cu and Cu_2O in this glass is consistent with mixed valence state for copper in the glasses as shown by the XANES experiments (Figure 5). The occurrence of Cu^I in the glass can be due to an incomplete reduction process from Cu^{II} to Cu^0 species which can led to the formation of Cu_2O crystalline phases during cooling of the melt. On the other hand, a partial oxidation process of the metallic Cu nanoparticles can also take place, leading to the formation of Cu-Cu_2O core-shell nanoparticles near to the surface of the glass.[26] The Scherrer equation[27] can be used for the calculation of grain size from FWHM (Full Width Half Maximum) and the position of the Cu^0 peak in XRD. However, the use of such an equation was not possible since the signal/noise ratio of XRD was very poor.

Figure 7 shows the electronic absorption spectra of the $x = 0.1$, 0.6 and 0.7 glasses. For blue glass ($x = 0.1$) no considerable absorption peak is observed in this region, while for brown glasses ($x = 0.6$ and 0.7) the localized surface plasmon resonance (LSPR) transition is clearly seen. When both are compared, the $x = 0.6$ glass present an absorption peak centered at 585 nm and the $x = 0.7$ glass shows a broader absorption band at around 605 nm.[26] Such LSPR bands are compatible with nanoparticles sizes with *ca.* tens of nanometers[28].

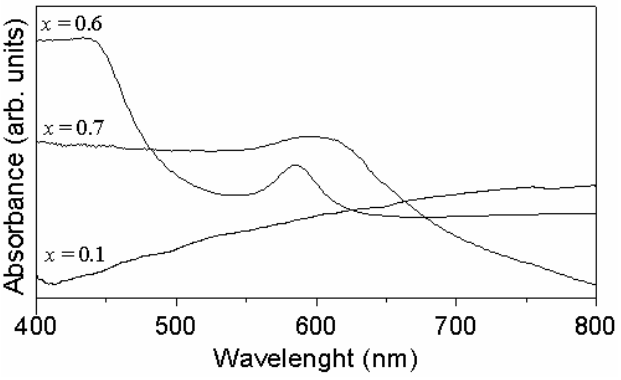

Figure 7. Electronic absorption spectra of the $(0.9\text{-}x)NaPO_3$ - xSb_2O_3- 0.1CuO glasses with different compositions.

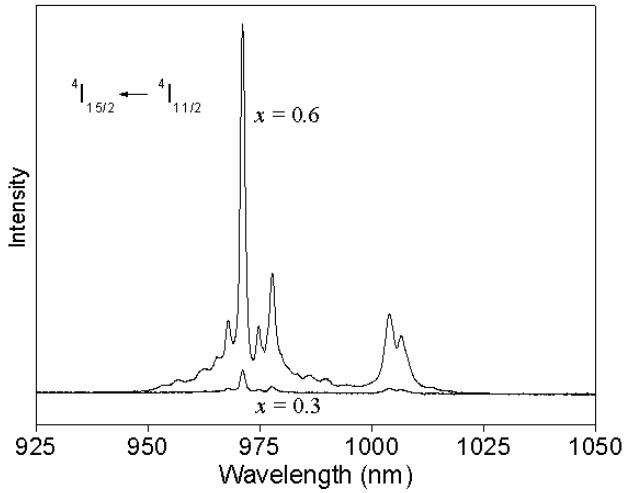

Figure 8. Fluorescence spectra of the Er^{III} doped glasses $(0.895\text{-}x)NaPO_3$-xSb_2O_3-0.1CuO-0.005Er_2O_3 with x = 0.3 and 0.6.

The broadening and red-shift of the LSPR band in the glass with higher antimony oxide concentration indicate with increasing the reducing agent content, average particle size becomes larger.[26,29] In this way we can consider that the control of the nanoparticle size is then possible via simple composition adjustments. It is noteworthy that the preclusion of the oxidation of the copper metallic nanoparticles imbedded in the glassy matrix for days after the synthesis is significantly important when compare with the low live time, just few minutes, of copper metallic surface in aqueous medium.[28]

The LSPR transition from copper nanoparticles found in these glasses motivated a new synthesis involving the doping of such glasses with RE ions. Figure 8 shows the fluorescence spectra of two glasses doped with 0.5Mol% of Er_2O_3: a sample with low reducing agent (Sb_2O_3) content: $(0.595)NaPO_3$-$0.3Sb_2O_3$-0.1CuO-$0.005Er_2O_3$; and another with high Sb_2O_3 concentration in the glass composition $(0.295)NaPO_3$-$0.6Sb_2O_3$-0.1CuO-$0.005Er_2O_3$. Both spectra show the fluorescence bands assigned to $^4I_{15/2} \leftarrow {}^4I_{11/2}$ transition of the Er^{III} ions in the glasses.[30] Even though both was recorded in the same accumulation conditions, a remarkable difference in their intensities (*ca.* 20x) can be observed. From these results it can be inferred that the presence of copper nanoparticles in the sample with x = 0.6, some of which in resonance with the exciting radiation, has to be the responsible for the enhancement of the fluorescence of the Er^{III} ion.[31] In the same way, the presence of the glassy matrix precludes the quenching of the fluorescence avoiding the physical contact between the Er^{III} ions and the metallic surface of copper.

Conclusions

The *Sb_2O_3 redox route* was used to obtain copper nanoparticles embedded in a glassy matrix, without the need of subsequent heat treatments. It was shown that the *size distribution of the copper particles can be tuned via controlled thermal conditions, such as melting temperature and time, cooling rate, etc.* The fast oxidation of the surface of copper nanoparticles, observed in aqueous medium can be precluded in such a glassy matrix. The Raman spectra of these composites showed that the short range structure around Sb atoms in the glassy matrix is similar to the high temperature β-Sb_2O_3 phase. This leads to the conclusion that antimony species present after melting synthesis at 1000°C underwent oxidative process into the glassy matrix. Therefore, through this synthetic route the control of the redox mechanism influences directly the structure, composition and, consequently, properties of the obtained glassy materials. In this way, it is of extreme importance to consider these phase changes processes as a main feature when discussing structure and properties of such glasses containing antimony oxide. It was shown that the control of the resonance of the surface plasmon from copper nanoparticles, obtained from its size distribution mediated by the Sb_2O_3 content, allow obtaining surface enhanced fluorescence, in the near infrared region, from Erbium (III) ion used as doping compound in such glasses. The method of obtaining copper nanoparticles during the preparation of glasses by the conventional melting/quenching technique, exploring the use of the reduction potential of antimony oxide during glass formation, without the need for subsequent heat treatments, is a yet to be explored field. In fact, glasses containing Sb_2O_3 as reduction agent were until now prepared only with silver and/or gold nanoparticles[20] but certainly a yet unknown number of metals and semi-metals can be reduced during the glass melting. It is clear that pure Au, Ag or Cu metallic particles, as well their combinations as core-shells and even alloys must be possible to be obtained via this antimony oxide redox route.

Acknowledgements

This work was financially supported by the Capes, CNPq and FAPEMIG (CEX-APQ-01468-09) Brazilian Funding Agencies. The Transmission Electron Microscopy images were supported by Instituto Nacional de Metrologia e Qualidade Industrial. The synchrotron experiments were supported by Brazilian Synchrotron Light Laboratory, Campinas – SP, Brazil.

Notes and references

[a]Núcleo de Espectroscopia e Estrutura Molecular – NEEM, Departamento de Química, Universidade Federal de Juiz de Fora, 36036-900 Juiz de Fora, MG, Brazil.

† Electronic supplementary information (ESI) available: Transmission Electron Microscopy Image of the $0.1NaPO_3$-$0.8Sb_2O_3$-0.1CuO glass prepared by Focused Ion Beam (FIB). DSC curves of the $(0.9\text{-}x)NaPO_3$-xSb_2O_3-0.1CuO glasses.

1 C. Noguez, *J. Phys. Chem. C*, 2007, **111**, 3806-3819.
2 A. J. Haes, C. L. Haynes, A. D. McFarland, G. C. Schatz, R. P. Van Duyne, S. L. Zou, *Mater. Res. Soc. Bull.* 2005, **30**, 368-375.

3 F. Gonella, P. Mazzoldi, Metal Nanocluster Composite Glasses. In *Handbook of Nanostructured Materials and Nanotechnology*, Nalwa, H. S., Ed.; Academic Press, San Diego, 2000, **4**, 81-158.
4 R. E. de Lamaestre, H. Bea, H. Bernas, J. Belloni, J. L. Marignier, *Phys. Rev. B* 2007**, 76**, 205431-1 – 18.
5 X. C. Yang, L. L. Li, M. Huang, J. F. Zhao, J. W. Hou, *J. Non-Cryst. Solids* 2011, **357**, 2301-2308.
6 Y. Teng, J. Zhou, F. Luo, G. Lin, J. Qiu, J. *J. Non-Cryst. Solids* 2011, **357**, 2380-2383.
7 I. Dmitruk, I. Blonskiy, I. Pavlov, O. Yeshchenko, A. Alexeenko, A. Dmytruk, P. Korenyuk, V. Kadan, *Plasmonics* 2009, **4(2)**, 115–119.
8 S. Chen, T. Akai, K. Kadono, T. Yazawa, *Chem. Commun.* 2001, **20**, 2090–2091.
9 A. Y. Zhang, T. Suetsugu, K. Kadono, *J. Non-Cryst. Solids* 2007, **353**, 44–50.
10 J. Shin, K. Jang, K. S. Lim, I. B. Sohn, Y. C. Noh, Lee, J. *Appl. Phys. A,* 2008, **93(4)**, 923–927.
11 G. Speranza, L. Minati, A. Chiasera, M. Ferrari, G. C. Righini, G. Ischia, *J. Phys. Chem. C* 2009, **113 (11)**, 4445–4450.
12 O. A. Yeshchenko, I. M. Dmitruk, A. M. Dmytruk, A. A. Alexeenko, *Mater. Sci. Engg. B* 2007, ***137*(1–3)**, 247–254.
13 G. Seifert, M. Kaempfe, K. J. Berg, H. Graener, *Appl. Phys. B,* 2000, **71 (6)**, 795–800.
14 L. R. P. Kassab, C. B. de Araújo, R. A. Kobayashi, R. A. de Pinto, D. M. da Silva, *J. Appl. Phys.* 2007, **102(10)**, 103515-1 – 4.
15 D. Lezal, J. Pedlikova, P. Kostka, J. Bludska, M. Poulain, J. Zavadil, *J. Non-Cryst. Solids* 2001, **284**, 288-295.
16 M. Nalin, Y. Messaddeq, S. J. L. Ribeiro, M. Poulain, V. Briois, G. Brunklaus, C. Rosenhahn, B. D. Mosel, H. Eckert, *J. Mater. Chem.* 2004, **14(23)**, 3398–3405.
17 S. E. Golunski, T. G. Nevell, M. I. Pope, *Thermochim. Acta,* 1981, **51**, 153-168.
18 J. Amador, E. Pueba Gutierrez, M. A. Monge, I. Rasines, C. Ruiz Valero, *Inorg. Chem.* 1988, **27**, 1367-1370.
19 E. I. Voit, A. E. Panasenko, L. A. Zemnukhova, *J. Struct. Chem.* 2009, **50(1)**, 60-66.
20 T. Som, B. Karmakar, *Nano Res.* 2009, **2**, 607-616.
21 M. Yin, C-K. Wu, Y. Lou, C. Burda, J. T. Koberstein, Y. Zhu, S.J. O'Brien, *Am. Chem. Soc.,* 2005, **127**, 9506-9511.
22 J. Massera, *J. Phys. Chem. Solids,* 2013, **74,** 121-127.
23 S. Mamedov, D. Stachel, M. Soltwisch, D. Quitmann, *J. Chem. Phys.* 2005, **123**, 124515-1 – 12.
24 L. B. Fletcher, J. J. Witcher, N. Troy, S. T. Reis, R. K. Brow, R. M. Vazquez, R. Osellame, D. M. Krol, *Opt. Mater. Express* 2011, **1(5)**, 845-855.
25 P. J. Durham, Theory of Xanes. In X-Ray Absorption: Principles, Applications, Techniques of EXAFS, SEXAFS and XANES; D. C. Koningsberger, R. Prins, Eds.; *Chemical analyses: A series of Monographs on Analytical Chemistry and its Applications*, John Wiley & Sons: New York, 1988, **92**, 53-84.
26 K. P. Rice, E. J. Jr. Walker, M. P. Stoykovich, A. E. Saunders, *J. Phys. Chem.,* 2011, **115**, 1793 – 1799.
27 A. Weibel, R. Bouchet, F. Boulc'h, P. Knauth, *Chem. Mater.*, 2005, **17**, 2378-2385.
28 D. F. de Carvalho, B. G. da Fonseca, I. L. Barbosa, S. M. Landi, L. A. de Sena, B. S. Archanjo, A. C. Sant'Ana, *Spectrochim. Acta*, Part A, 2013, **103**, 108-113.
29 K. E. Lipinska-Kalita, D. M. Krol, R. J. Hemley, G. Mariotto, P. E. Kalita, Y. Ohki, *J. Appl. Phys.,* 2005, **98**, 054301-1 – 6.
30 N. Jaba, H. B. Mansour, B. Champagnon, *Opt. Mater.*, 2009, **31**, 1242-1247.
31 L. R. P. Kassab, C. B. de Araújo, R. A. Kobayashi, R. A. Pinto, D. M. Silva, *J. Appl. Phys.*, 2007, **102**, 103515.

The Sb_2O_3 redox route to obtain copper nanoparticles in glasses with plasmonic properties

Douglas F. Franco, Antonio C. Sant'Ana, Luiz F. C. De Oliveira and Mauricio A. P. Silva*

Núcleo de Espectroscopia e Estrutura Molecular – NEEM, Departamento de Química, Universidade Federal de Juiz de Fora, 36036-900 Juiz de Fora, MG, Brazil.

Production of oxide glasses containing Cu^{II}, Cu^{I} and Cu^{0} nanoparticles by redox process during melting without subsequent thermal treatment.

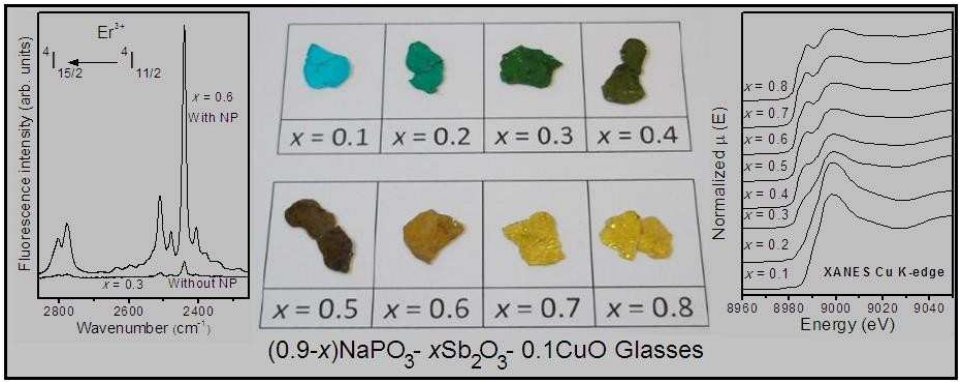

Graphical Abstract